Vacuum-UV fluorescence spectroscopy of PF3 in the range 9–20 eV

Biehl, H.; Boyle, Kenneth; Seccombe, D. P.; Tuckett, R. P.; Baumgärtel, H.; Jochims, H. W.

DOI:
10.1063/1.475449

Vacuum-UV fluorescence spectroscopy of PF_3 in the range 9–20 eV

H. Biehl, K. J. Boyle, D. P. Seccombe, and R. P. Tuckett
School of Chemistry, University of Birmingham, Edgbaston, Birmingham B15 2TT, United Kingdom

H. Baumgärtel and H. W. Jochims
Institut fur Physikalische und Theoretische Chemie, Freie Universitat Berlin, Takustrasse 3, 14195 Berlin, Germany

(Received 13 August 1997; accepted 9 October 1997)

The vacuum-UV and visible spectroscopy of PF_3 using fluorescence excitation and dispersed emission techniques is reported. The fluorescence excitation spectrum has been recorded following photoexcitation with monochromatized synchrotron radiation from the Daresbury, UK source in the energy range 9–20 eV with an average resolution of ~ 0.015 eV. Transitions to the three lowest-energy bands in the Rydberg spectra show resolved vibrational structure, they are assigned to transitions to the $(8a_1)^{-1}$ $4p$, $5p$, and $6p$ Rydberg states of PF_3, and fluorescence is due to valence transitions in the PF_2 radical. From a Franck–Condon analysis of the vibrational structure, it is shown that the FPF bond angle in PF_3 increases by $\sim 14 \pm 1°$ upon photoexcitation. The use of optical filters shows that at least three excited electronic states of PF_2 are responsible for the induced emission. Dispersed emission spectra in the UV/visible region have been recorded with an optical resolution of 8 nm at the BESSY 1, Germany synchrotron source at the energies of all the peaks in the excitation spectrum. Four different decay channels are observed: (a) PF_2 $\tilde{A}\,^2A_1 - \tilde{X}\,^2B_1$ fluorescence in the wide range 320–550 nm for photon energies around 9.8 eV, (b) PF_2 $\tilde{A} - \tilde{X}$, and $\tilde{B}\,^2B_2 - \tilde{X}\,^2B_1$ fluorescence at ~ 300 nm for photon energies around 11.0 eV, (c) PF_2 $\tilde{C}\,^2A_1 - \tilde{X}\,^2B_1$ and $\tilde{E}\,^2B_1$ $(^2\Pi) - \tilde{A}\,^2A_1$ fluorescence at ~ 222 and 325 nm, respectively, for photon energies around 14.4 eV, and (d) PF $A\,^3\Pi - X\,^3\Sigma^-$ fluorescence between 300–380 nm for photon energies around 16.1 eV. These assignments are confirmed by action spectra in which the excitation energy of the vacuum-UV radiation is scanned with detection of the fluorescence at a fixed, dispersive wavelength. Using the single-bunch mode of the BESSY 1 source, we have attempted to measure the lifetimes of the emitting states, but the timing profile of the source imposes an upper limit on lifetimes that can be measured of ~ 500 ns. We have therefore only been able to measure values for the bent $\tilde{C}\,^2A_1$ and linear $\tilde{E}\,^2B_1$ $(^2\Pi)$ states of PF_2 of 14.7 and 7.9 ns, respectively; the lifetimes of the other emitters are too long to measure by this method. Our assignments in PF_2 are heavily dependent on recent *ab initio* calculations on the geometries and energies of the valence electronic states of this species. Our knowledge on the electronic spectroscopy of this free radical is reviewed.
 [S0021-9606(98)01603-1]

I. INTRODUCTION

In a series of papers[1–4] we have reported the observation and analysis of the nondispersed vacuum ultraviolet (UV) fluorescence and dispersed emission spectra following vacuum-UV excitation of a range of polyatomic molecules in the gas phase. Experiments are performed at excitation energies in the range 8–25 eV, with complementary experiments being performed at the Daresbury, UK and BESSY 1, Germany synchrotron sources. To date we have performed experiments on group III and IV halides such as BCl_3,[1] BBr_3,[2] CF_3X (X=F, Cl, Br, H),[3] and SiF_4.[4] Many of these compounds are either widely used or are indirectly involved in the radiofrequency plasma etching of semiconductor devices. The use of vacuum-UV photons affords a more controllable method of excitation than low-energy plasma electrons covering the same energy range. In this paper we report the results of a comprehensive study of fluorescence processes following vacuum-UV photoexcitation of PF_3, one of the simplest group V halides. Preliminary results from this study were published recently.[5]

The ground state of PF_3 has a pyramidal structure with C_{3v} symmetry. With the numbering scheme including core orbitals, the electron configuration of the valence molecular orbitals (MOs) have symmetry labels and occupancies $\cdots(6a_1)^2(4e)^4(7a_1)^2(5e)^4(6e)^4(1a_2)^2(8a_1)^2$. The $8a_1$ highest-occupied MO is essentially a lone-pair orbital located on the phosphorus atom with 35% P $3s$ and 35% P $3p_z$ character.[6] The most recent direct determination of the structure of PF_3 by gas-phase electron diffraction yielded $\vartheta_{FPF} = 97.8 \pm 0.2°$ and $R_{P-F} = 1.570 \pm 0.005$ Å.[7] There have been several photoionization studies of PF_3, most notably by He I photoelectron spectroscopy,[8] by He I photoelectron–photoion coincidence spectroscopy,[9] and by pseudo-photon $(e,e+\text{ion})$ dipole spectroscopy.[10] The vertical ionization potentials (IP) of the ground and excited valence states of PF_3^+ are given in Table I. Of most importance to this work, our preliminary study established that the $\tilde{X}\,^2A_1$ ground state of PF_3^+ and the Rydberg states converging to this ionic state also have C_{3v} symmetry with an increased bond angle of $112 \pm 1°$, a vibrational wavenumber of the ν_2 umbrella mode

TABLE I. Energetics and dissociation channels of PF_3 and PF_3^+.

Neutral/parent ion		Dissociation channel	Dissocation energy (0 K)/eV	Vertical (adiabatic) IP/eV[a]
PF_3^+	$\tilde{F}\ ^2A_1$			22.55
		$PF^+ + 2F$	20.5	
	$\tilde{E}\ ^2E$			19.50
		$PF^+ + F_2$	18.85	
	$\tilde{D}\ ^2A_1$			18.60
	$\tilde{C}\ ^2E$			17.46
	$\tilde{B}\ ^2E$			16.30
	$\tilde{A}\ ^2A_2$			15.88
		$PF_2^+ + F$	14.48	
	$\tilde{X}\ ^2A_1$			12.25 (11.57)
		PF $g\ ^1\Pi + 2F$	17.46[b]	
		PF $d\ ^1\Pi + 2F$	15.47	
		PF $A\ ^3\Pi + 2F$	14.68	
		PF $X\ ^3\Sigma^- + 2F$	11.00	
		PF $g\ ^1\Pi + F_2$	15.81	
		PF $d\ ^1\Pi + F_2$	13.82	
		PF $A\ ^3\Pi + F_2$	13.03	
		PF $X\ ^3\Sigma^- + F_2$	9.35	
		$PF_2\ \tilde{G}\ ^2A_2 + F$	13.33[c]	
		$PF_2\ \tilde{F}\ ^2A_2 + F$	13.11	
		$PF_2\ \tilde{E}\ ^2B_1 + F$	11.95	
		$PF_2\ \tilde{b}\ ^4A_2 + F$	11.85	
		$PF_2\ \tilde{D}\ ^2B_2 + F$	11.85	
		$PF_2\ \tilde{C}\ ^2A_1 + F$	11.07	
		$PF_2\ \tilde{a}\ ^4B_1 + F$	9.41	
		$PF_2\ \tilde{B}\ ^2B_2 + F$	8.81	
		$PF_2\ \tilde{A}\ ^2A_1 + F$	7.94	
		$PF_2\ \tilde{X}\ ^2B_1 + F$	5.65	
PF_3	$\tilde{X}\ ^1A_1$			0

[a]Reference 8.
[b]References 14 and 21.
[c]T_e values for the energies of the excited states of PF_2 from Ref. 18.

of $454 \pm 24\ cm^{-1}$, and a barrier to planarity of 2.08 eV.[5] There have been fewer studies of the excited (Rydberg) states of neutral PF_3, the only three studies of note being a photographic vacuum-UV absorption study of the two lowest Rydberg states over thirty years ago,[11] a measurement of absolute optical densities in absorption in the 5–10 eV range,[12] and a very recent pseudo-photon (e,e) study up to 23 eV at a resolution of ~ 0.05 eV.[10] Humphries *et al.*[11] resolved vibrational structure in two of the Rydberg transitions with band origins of 1405 and 1212 Å (8.82 and 10.22 eV, respectively), but the electronic transitions could not be assigned because accurate IPs for the valence MOs of PF_3 were not known at the time. Surprisingly, there have been no absorption studies in the vacuum-UV using tunable synchrotron radiation.

We have performed fluorescence experiments on PF_3 in the vacuum-UV energy range of 8–25 eV, and peaks are observed below the adiabatic IP of 11.57 eV.[8] The emitters of the fluorescence must therefore either be PF_3 itself or a neutral fragment, such as PF_2 or PF, produced by photodissociation of Rydberg states of PF_3. Experience from previous studies[1–4] suggests that photodissociation of Rydberg states of polyatomic molecules is a very rapid process, and therefore fluorescence is invariably associated with a neutral fragment and not the parent molecule. The energies of the $PF_2 + F$, $PF + F_2$, and $PF + 2F$ dissociation channels of PF_3 are calculated from the 0 K heats of formation of PF_x ($x = 1-3$) to be 5.65, 9.35, and 11.00 eV, respectively.[13] The valence electronic spectroscopy of PF is well understood,[14,15] and the energies of the possible emitting states of PF are shown in Table I. By contrast, the electronic spectroscopy of the PF_2 free radical is very poorly characterized, there being only one observation of a vibrationally resolved spectrum in the UV/visible region.[16] Furthermore, the assignment of this spectrum has been queried by some theoretical studies.[17–19] The topic is reviewed in Sec. III. At this stage we note that of four *ab initio* studies that have been carried out in recent years on the positions and geometries of the excited states of this radical,[17–20] we have chosen the results of Latifzadeh and Balasubramanian,[18] displayed in the thermochemistry of Table I, to show the energies of possible emitting states of the PF_2 radical.

Section II describes the experimental techniques, and Sec. III reviews the spectroscopy of the PF_2 radical. Section IV states the results we have obtained, which are analyzed and discussed in Sec. V. Conclusions are drawn in Sec. VI.

II. EXPERIMENT

The experiments were performed at two synchrotron sources. Nondispersed, vacuum-UV fluorescence excitation spectra of PF_3 were recorded at the UK source at Daresbury. A 5 m normal-incidence McPherson monochromator (range 8–25 eV, best resolution 0.01 nm) attached to the 2 GeV electron storage ring was used as the primary source of tunable radiation. Dispersed fluorescence and vacuum-UV ''action'' spectra of PF_3 were performed at the BESSY 1 storage ring in Berlin. Now a 1.5 m normal-incidence monochromator (range also 8–25 eV, optimum resolution 0.03 nm) attached to the 800 MeV electron storage ring was used to monochromatise the radiation. Using the single-bunch mode of the synchrotron, lifetime measurements were made at both sources. The ability of the Berlin facility to disperse the fluorescence at a fixed emission wavelength has made this a preferable source for such experiments. This dispersion enables the identity and the electronic state of the emitting species to be defined.[4]

At Daresbury, monochromatized synchrotron radiation entered the interaction region through a 2 mm i.d., 500 mm long glass capillary. The differential pumping provided by the capillary ensured that experiments could be performed ''windowless'' at wavelengths below the lithium fluoride cutoff of ~ 105 nm. The fluorescence produced from a sodium salicylate coated pyrex window located behind the interaction region was used to monitor the vacuum-UV photon flux for normalization purposes. Second-order radiation has been estimated to contribute $\sim 10\%$ of the flux for photon energies below 13 eV on this McPherson monochromator.[22] The photon beam crossed an effusive spray of PF_3 (background pressure $\sim 10^{-4}$ Torr) which originated from a long hyperdermic needle of i.d. 0.5 mm. Fluorescence induced at

the intersection region was focused through a Spectrocil B quartz window by an aluminium-coated $f=75$ mm spherical concave mirror onto an EMI 9813 QB photomultiplier tube (range $\sim 190-650$ nm) maintained at 298 K. Optical filters can be inserted in front of the photomultiplier tube to isolate different emission bands. The tube was operated in the photon counting mode, and signal pulses were shaped using a constant fraction differential discriminator (Ortec 583). Fluorescence excitation spectra were recorded at a typical resolution of 0.1 nm (~ 0.01 eV at 11 eV) using the multibunch mode of the synchrotron. The signals from the photomultiplier tube and the sodium salicylate window were passed to a personal computer via a CAMAC interface. Spectra were normalized to the vacuum-UV flux, and the background fluorescence subtracted.

In Berlin, synchrotron radiation passed from the primary monochromator through a small chamber and into a brass cube (side 20 mm). The chamber and cube, separated by a 1 mm slit to aid differential pumping, were pumped by different turbo-molecular pumps. A removable lithium fluoride window could be positioned prior to the exit slit of the monochromator. PF_3 vapor effused into the interaction region which is separated from the cube by a 0.5 mm slit, giving a typical pressure in the cube of $\sim 2\times 10^{-5}$ Torr; the pressure within the interaction region was higher, although it was not possible to measure directly. The induced fluorescence was dispersed by a 20 cm focal length monochromator (Jobin Yvon H20UV or H20VIS). This secondary monochromator had no entrance slit, and a fixed exit slit giving a reciprocal dispersion of 4 nm mm^{-1}. Fluorescence was detected by a red-sensitive Hamamatsu R6060 photomultiplier tube water cooled to ~ 280 K. The effective range of the H20UV monochromator was then 190 to ~ 500 nm, of the H20VIS 190 to ~ 600 nm. In the multibunch mode the following three experiments were possible. First, fluorescence excitation spectroscopy, in which the secondary monochromator was set to zero order and the primary monochromator was scanned; in practice, this experiment was only used to confirm a similar spectrum obtained at higher resolution at Daresbury. Second, action spectroscopy, in which the secondary monochromator was set to a specific fluorescence wavelength and the primary monochromator was scanned. Third, dispersed fluorescence spectroscopy, in which the induced fluorescence was dispersed for a fixed photoexcitation energy between 9 and 20 eV. The scanning of both monochromators and the data collection were controlled using a personal computer. Neither the action nor the dispersed spectra were normalized to the sensitivity curves of the primary or secondary monochromators, respectively. Both monochromators were calibrated using the N_2^+ $B\ ^2\Sigma_u^+ - X\ ^2\Sigma_g^+$ (0,0) emission band at 391 nm with production threshold of 18.76 eV.[21] In the single-bunch mode, lifetimes of the emitting states were measured in the following manner. The VUV excitation wavelength (λ_1) and the emission wavelength (λ_2) were defined. After shaping and discrimination, fluorescence pulses from the Hamamatsu photomultiplier tube (rise time ~ 1.5 ns) were used as the start signal for a time-to-amplitude converter (Ortec 567). The synchrotron bunch marker (20 ps pulses every 208 ns, the transit time of electrons around the storage ring) was used as the stop signal. The resulting decay data were collected in real time using a multichannel analyser card mounted in a 386 personal computer. An absolute time calibration was provided by a time calibrator (Ortec 462). The lifetime of the $B\ ^2\Sigma_u^+$ state of N_2^+ has been measured to be 60 ± 1 ns. This value is in good agreement with that given in the literature,[21] confirming that collisional quenching makes no contribution to the rate of decay of the fluorescence signal for shorter lifetimes at the pressures used in these experiments.

Some lifetime data were recorded with the single-bunch mode at Daresbury (200 ps pulses every 320 ns). A Mullard 2254 B red-sensitive photomultiplier tube cooled to 250 K was used with similar electronics to those utilised in the BESSY 1 experiments. The main advantage of this apparatus compared to that used in Berlin is that it is more sensitive to visible radiation with $\lambda > \sim 450$ nm. In theory, the Daresbury experiment can also measure slightly longer lifetimes because of the longer time between pulses at the UK source. In practice, however, the ability to disperse the induced fluorescence at Berlin is much more beneficial, and it is only the BESSY 1 results that are presented. Unlike our recent SiF_4 study,[4] parent ion emission was not observed with PF_3. The problems of second-order radiation from the primary monochromator causing fluorescence from PF_3^+ at the same apparent energy as much weaker fluorescence from PF_2 or PF produced by photodissociation of Rydberg states of PF_3 in first order did not therefore arise.

The lifetime data were analyzed using a nonlinear least-squares program, FLUOR,[23] developed by staff at Daresbury. The measured fluorescence signal is not a simple decay, but is a convolution of the fluorescence decay with a ''prompt'' instrument component, plus a background. The prompt component is the average time profile of the single bunch in the storage ring convoluted with the response time of the photomultiplier tube and the associated detection electronics. The signal observed with no gas present, arising from scattering of the synchrotron radiation, offers a reasonable approximation to the prompt component of the measured fluorescence. This ''prompt signal'' was measured prior to the lifetime decays for PF_3 at BESSY 1. The scattered light was maximized by setting both monochromators to zero order, i.e., $\lambda_1=\lambda_2=0$. A model, either the sum of one or two exponential functions, was chosen to represent the time behavior of the fluorescence. The choice of model was dependent upon whether one or two emissions were being excited at a particular excitation wavelength λ_1, and whether λ_2 was set to zero order or not. The model function could then be convoluted with the prompt signal and fitted to the experimental data by minimizing the Poisson-weighted sum of the squares of the residuals. This enabled experimental values of the lifetimes (τ_1,τ_2), amplitudes (A_1,A_2), and the background (B) to be obtained, where

$$y=A_1.\exp(-t/\tau_1)+A_2.\exp(-t/\tau_2)+B.$$

If the decay times are very much longer than the duration of the prompt signal, it is possible to use a model function

without this convolution procedure. However, since the lifetimes of emitting states that we measure for PF_2 are all less than ~ 20 ns and the response time of the photomultiplier tube is as long as 1.5 ns, we found it necessary to deconvolute the prompt signal from our lifetime data. We used this fitting procedure satisfactorily for the first time in our SiF_4 study.[4]

III. THE ELECTRONIC SPECTROSCOPY OF THE PF_2 AND PF RADICALS

As we show in Sec. IV and have commented previously,[5] peaks are observed in the fluorescence excitation spectrum of PF_3 with resolved vibrational structure at photon energies below 12 eV. The threshold energy for producing the lowest fluorescing state of PF is 13.03 eV (Table I). Therefore PF can be discounted as the emitter. The use of filters has shown that fluorescence predominantly occurs in the visible region but with a substantial UV component. Since there are no valence states of PF_3 which lie ~ 3 to 4 eV below the energies of its lowest Rydberg states, the emitter can only be the PF_2 radical. It is therefore pertinent to review our knowledge about the excited electronic states and electronic spectroscopy of this radical.

The equilibrium structure of the ground state of PF_2 has been accurately determined by microwave spectroscopy ($\vartheta = 98.5°$, $R_{P-F} = 1.579$ Å), and the vibrational wavenumbers of its three normal modes inferred from the centrifugal distortion data ($\nu_1 = 864$, $\nu_2 = 365$, $\nu_3 = 848$ cm^{-1}).[24] ν_1 and ν_3 have been observed directly by matrix isolation spectroscopy to be 831 and 852 cm^{-1}, respectively.[25] There have been only two experimental studies of the electronic spectroscopy of this radical. First, Rydberg states in the wave number range 50 000–70 000 cm^{-1} have been characterized by two-photon resonance enhanced multiphoton ionization spectroscopy.[26] By simulation of the rotational band contors, the geometry of those states converging on the $\tilde{X}\ ^1A_1$ ground state of PF_2^+ has been determined ($\vartheta = 109°$, $R_{P-F} = 1.49$ Å), and the ionization potential determined is in good agreement with He I photoelectron and photoionization mass spectroscopy data.[27,28] Second, there has been one observation between 420 and 520 nm by dispersed emission spectroscopy of a valence transition in the PF_2 radical.[16] The PF_2^* was formed by passing a PF_3/Ar mixture through a dc discharge and observing the emission a long distance downstream. Mainly on account of the perceived long lifetime of the emitter (>10 ms), Zhao and Setser (ZS) assigned this to a spin–forbidden transition, and obtained values for ν_1 (symmetric stretch) and ν_2 (bending mode) in both electronic states. The ground state values ($\nu_1'' = 841$, $\nu_2'' = 367$ cm^{-1}) were in excellent agreement with the value from the matrix work of Burdet *et al.*[25] for ν_1 and the inferred value of Saito *et al.*[24] for ν_2, confirming that PF_2 was indeed the emitter. The upper state values ($\nu_1' = 505$, $\nu_2' = 220$ cm^{-1}) were substantially reduced from those in the ground state. Following Walsh[29] and using a numbering scheme which includes the P $1s$ $2s$ $2p$, and F $1s$ core orbitals, the electron configuration of the valence orbitals of PF_2 in its ground electronic state is $\cdots(5a_1)^2(3b_2)^2(6a_1)^2(4b_2)^2(2b_1)^2(7a_1)^2(8a_1)^2(1a_2)^2(5b_2)^2(3b_1)^1(9a_1)^0(6b_2)^0$. The $3b_1$ highest-occupied molecular orbital (MO) is essentially the antibonding combination of atomic orbitals on P $3p_x$ and two F $2p_x$, where the x axis lies perpendicular to the plane of the radical. Zhao and Setser believed that the first excited state of quartet symmetry should arise from excitation of a $5b_2$ electron to the $9a_1$ lowest-unoccupied MO, giving rise to the $\tilde{a}\ ^4A_2$ state. They assigned the observed emission to the spin–forbidden $\tilde{a}\ ^4A_2 - \tilde{X}\ ^2B_1$ transition.

Zhao and Setser's paper has stimulated four very recent theoretical studies on the properties of excited valence states of the PF_2 radical.[17–20] Johnson and Irikura (JI)[17] calculated the energies of states below 40 000 cm^{-1} using complete active space self-consistent field (CASSCF) techniques refined by second-order perturbation theory. Geometries and vibrational frequencies were calculated for all states at the CASSCF (3,8)/6-311 level. Latifzadeh and Balasubramanian (LB)[18] used CASSCF followed by multireference single and double configuration interaction methods that included up to 1.2 million configurations. Energies and geometries of both bent and linear excited states of PF_2 with both doublet and quartet spin symmetry up to 62 000 cm^{-1} were reported. The P–F bond length was optimized at each value of the FPF bond angle. While the results for the bending potential curves are essentially similar to those of the JI study, there are some significant differences which have been explained by the fact that these preliminary JI calculations were all performed at a fixed P–F bond length (1.584 and 1.600 Å for the doublet and quartet states, respectively). A less complete study by Cai[20] calculated the energies, geometries and vibrational frequencies of the first electronic states of $^2B_1$, $^2A_1$, $^2B_2$, and $^2A_2$ symmetry. This study assumed C_{2v} geometry, linear states of PF_2 were not calculated, and so there is not an immediate match between the states calculated by either JI or LB and those calculated by Cai. Unlike the other three *ab initio* studies, however, Cai reports calculations of the electronic transition moment of the dipole-allowed $^2A_1 - \tilde{X}\ ^2B_1$ and $^2A_2 - \tilde{X}\ ^2B_1$ transitions, and hence radiative lifetimes of these $^2A_1$ and $^2A_2$ excited states. He comments that the $^2B_2 - \tilde{X}\ ^2B_1$ transition is dipole-forbidden. A resumé of the results of these three papers is given in Table II, and we comment that there is no match between these valence states of PF_2 and the two lowest Rydberg states of $^2B_1$ and $^2A_1$ symmetry between 52 000 and 55 000 cm^{-1} observed in the REMPI study.[26] Finally, Lee *et al.*[19] simulate the Franck–Condon intensity distribution of the $\tilde{B}\ ^2B_2(\nu_1', \nu_2') - \tilde{X}\ ^2B_1(\nu_1'', \nu_2'')$ transition, using *ab initio* potential-energy curves calculated at the MP2/6-311G($2df$) level.

There seems to be general agreement that the assignment of the band with origin 421 nm observed by ZS to $\tilde{a}\ ^4A_2 - \tilde{X}\ ^2B_1$ is incorrect, in that the lowest quartet state is calculated by both JI and LB to be of B_1, not A_2, symmetry. Furthermore, this $^4B_1$ state is calculated to be linear, and therefore would give a very much wider Franck–Condon envelope in a transition to the highly bent $\tilde{X}\ ^2B_1$ ground state

TABLE II. Energies (T_e/cm^{-1}), geometries, and vibrational wavenumbers of the ground and excited valence electronic states of the PF_2 free radical predicted by theory.

Electronic state	CASSCF +MRSDCI (Cai)[a]	CASSCF +MRSDCI	R_{P-F} /Å	ϑ_{FPF} /°	CASSCF	CASSCF +PT2	R_{P-F} /Å	ϑ_{FPF} /°	ν_1[d]	ν_2[d]	ν_3[d]	Predominant e^- excitation (JI)[c]
		←(LB)[b]→				←(JI)[c]→			←/cm^{-1}→			
$\widetilde{X}\ ^2B_1$[e]	0	0	1.61	97.5	0	0	1.58	98.5	849	372	825	
$\widetilde{A}\ ^2A_1$		18 502	1.66	177	20 278	15 798	1.63	173	565	336	670	$9a_1 \leftarrow 3b_1$
$\widetilde{B}\ ^2B_2$		25 487	1.64	83	26 102	21 791	1.59	85	773	471	545	$6b_2 \leftarrow 3b_1$
$\widetilde{C}\ ^2A_1$	45 594	43 707	1.60	110	48 852	40 304	1.58	125	727	300	881	$3b_1 \leftarrow 8a_1$
$\widetilde{D}\ ^2B_2$	53 038	50 006	1.83	62					795[a]	460[a]	649[a]	$3b_1 \leftarrow 5b_2$
$\widetilde{E}\ ^2B_1$		50 812	1.67	180	52 992	41 596	1.62	180	537	447	627	$9a_1 \leftarrow 8a_1$
$\widetilde{F}\ ^2A_2$		60 168	2.05	180								
$\widetilde{G}\ ^2A_2$	63 338	61 935	1.84	77	74 774		1.83	74	775[a]	375[a]	699[a]	$3b_1 \leftarrow 1a_2$
$\widetilde{a}\ ^4B_1$		30 286	1.66	180	32 963	27 528	1.63	180	572	335	655	$10a_1 \leftarrow 8a_1$
$\widetilde{b}\ ^4A_2$		50 046	1.67	87	51 527	46 879	1.59	89	545	305	743	$7b_2 \leftarrow 8a_1$

[a]Reference 20.
[b]Reference 18.
[c]Reference 17.
[d]Reference 17, unless otherwise stated.
[e]Experimental values for the geometry of the $\widetilde{X}\ ^2B_1$ (000) state of PF_2 are $R_{P-F}=1.579$ Å and $\vartheta_{FPF}=98.5°$ (Ref. 24). From the observed centrifugal distortion constants, Saito *et al.* (Ref. 24) estimate $\nu_1=864$, $\nu_2=365$, and $\nu_3=848$ cm^{-1}. Zhao and Setser (Ref. 16) observe $\nu_1=841$ and $\nu_2=367$ cm^{-1}. Burdet *et al.* (Ref. 25) measure $\nu_1=831$ and $\nu_3=852$ cm^{-1}.

than is observed. Both JI and LB assign this band to the dipole-forbidden $\widetilde{B}\ ^2B_2-\widetilde{X}\ ^2B_1$ transition, the forbidden nature of the transition explaining the anomalous long lifetime measured by ZS. Lee *et al.* show fairly convincingly that there is good agreement between the vibrational structure observed by ZS and that calculated by their Franck–Condon analysis of the $\widetilde{B}-\widetilde{X}$ transition. Furthermore, their calculated spectrum is fairly sensitive to the geometry of the $\widetilde{B}\ ^2B_2$ state, and they are able to deduce a geometry for this state of $R_{P-F}=1.63\pm0.01$ Å and $\vartheta=84.9\pm0.2°$. These values are in excellent agreement with those calculated by the two more extensive *ab initio* studies,[17,18] especially those of LB. However, these theoretical studies are not able to explain totally satisfactorily one aspect of the ZS spectrum. The JI calculations predict values for ν_1 and ν_2 in the $\widetilde{B}\ ^2B_2$ state (773 and 471 cm^{-1}) much greater than those observed (505 and 220 cm^{-1}). Their explanation is to re-assign the bands involving ν_1' and ν_2', such that ν_1' is reassigned to ν_2' and ν_2' is reassigned as sequence bands of the symmetric stretch, i.e., 1_1^1, 1_2^2, etc. Lee *et al.*[19] also comment that they are not able to simulate or predict the 220 cm^{-1} experimental observation of ZS. It should be noted that the near-linear first excited state of PF_2, $\widetilde{A}\ ^2A_1$, has predicted vibrational wavenumbers for ν_1 and ν_2 (565 and 336 cm^{-1})[17] much closer to the experimental observations, although our belief is that this is coincidental. Whilst the reassignment by JI, LB and Lee *et al.* of the 421 nm band to the $\widetilde{B}-\widetilde{X}$ transition is almost certainly correct, we believe that under our very different experimental conditions for producing PF_2^* the $\widetilde{A}\ ^2A_1-\widetilde{X}\ ^2B_1$ band is observed at comparable wavelengths in our spectra (see Sec. V).

In Sec. IV we show that peaks observed in the fluorescence excitation spectrum of PF_3 with photon energies below 15 eV suggest that fluorescence is being observed from a minimum of four different excited states of the PF_2 radical. Since theory is leading experiment in our understanding of the valence electronic spectroscopy of PF_2, our assignment of these transitions is critically dependent on the predictions of these *ab initio* studies.[17–20] In Table III, we show the equilibrium wavelengths, λ_e, at which transitions between the different electronic states of PF_2 are predicted to occur in the UV/visible region. The table also shows the energy of the excited electronic state of PF_2 above the ground state of PF_3, and the change in R_{P-F} and ϑ_{FPF} for the PF_2 electronic transition. The calculated change in bond angle is perhaps more significant, because a large value of $|\Delta\vartheta|$ should manifest itself as a very broad Franck–Condon envelope in the electronic band. Conversely, a relatively narrow band in a dispersed emission spectrum is unlikely to occur for an electronic transition in which either $|\Delta R|$ or $|\Delta\vartheta|$ is large.

The electronic spectroscopy of PF is much better characterized, both by experiment and by *ab initio* calculations.[14,15] The ground and first two excited states ($X\ ^3\Sigma^-$, $a\ ^1\Delta$, and $b\ ^1\Sigma^+$) have the $\pi^4\sigma^2\pi^{*2}$ electron configuration characteristic of $(np)^8$ diatomic molecules such as O_2 and NF. The first excited valence states ($A\ ^3\Pi$ and $d\ ^1\Pi$) both arise from the electron configuration $\pi^4\sigma^1\pi^{*3}$, whilst the next excited bound singlet state, $g\ ^1\Pi$, is probably a Rydberg state. The $A-X$, $d-a$, $d-b$, $g-a$, and $g-b$ transitions were first characterized in emission at rotational resolution by Douglas and Frackowiak,[14] and the energies of the singlet relative to the triplet states were determined by observation of the spin–forbidden $b-X$ transition at 748 nm by Colin *et al.*[30] The radiative lifetimes of the $A\ ^3\Pi$, $b\ ^1\Sigma^+$, and $d\ ^1\Pi$ states have recently been measured by Setser *et al.*[31,32] to be 4.2 ± 0.2 μs (for $v_A'=0$), 9.7 ± 1.2 ms, and 0.96 ± 0.05 μs (for $v_d'=0$), respectively. The lifetimes of the $a\ ^1\Delta$ and $g\ ^1\Pi$ states have not been reported.

TABLE III. Equilibrium wavelengths (λ_e/nm) of all possible electronic transitions in the UV/visible region (160–700 nm) for the PF_2 radical predicted by theory.

Transition	E'/eV[a]	$\Delta\vartheta$/° (LB)[b]	ΔR/Å (LB)[b]	CASSCF +MRSDCI (Cai)[c]/nm	CASSCF +MRSDCI (LB)[b]/nm	CASSCF (JI)[d] /nm	CASSCF +PT2 (JI)[d]/nm	τ'
$(\tilde{X}\ ^2B_1)$	5.65							
$\tilde{A}\ ^2A_1-\tilde{X}\ ^2B_1$	7.94	+80	+0.05		540	493	633	
$\tilde{B}\ ^2B_2-\tilde{X}\ ^2B_1$[e]	8.81	−14	+0.03		392	383	459	11 ms[f]
$\tilde{C}\ ^2A_1-\tilde{X}\ ^2B_1$	11.07	+12	−0.01	219	229	205	248	16 ns[c]
								14.7 ns[g]
$\tilde{D}\ ^2B_2-\tilde{X}\ ^2B_1$[e]	11.85	−35	+0.22	189	200			long[c]
$\tilde{D}\ ^2B_2-\tilde{A}\ ^2A_1$		−115	+0.17		317			
$\tilde{D}\ ^2B_2-\tilde{B}\ ^2B_2$		−21	+0.19		408			
$\tilde{E}\ ^2B_1-\tilde{X}\ ^2B_1$	11.95	+82	+0.06		197	189	240	7.9 ns[g]
$\tilde{E}\ ^2B_1-\tilde{A}\ ^2A_1$		+3	+0.01		310	306	388	
$\tilde{E}\ ^2B_1-\tilde{B}\ ^2B_2$[e]		+97	+0.03		395	372	505	
$\tilde{F}\ ^2A_2-\tilde{X}\ ^2B_1$	13.11	+82	+0.44		166			
$\tilde{F}\ ^2A_2-\tilde{A}\ ^2A_1$[e]		+3	+0.39		240			
$\tilde{F}\ ^2A_2-\tilde{B}\ ^2B_2$		+97	+0.41		288			
$\tilde{G}\ ^2A_2-\tilde{X}\ ^2B_1$	13.33	−20	+0.23	158	161	134		8 ns[c]
$\tilde{G}\ ^2A_2-\tilde{A}\ ^2A_1$[e]		−100	+0.18		230	183		
$\tilde{G}\ ^2A_2-\tilde{B}\ ^2B_2$		−6	+0.20		274	205		
$\tilde{a}\ ^4B_1-\tilde{X}\ ^2B_1$	9.41	+82	+0.05		330	303	363	
$\tilde{b}\ ^4A_2-\tilde{X}\ ^2B_1$	11.85	−10	+0.06		200	194	213	
$\tilde{b}\ ^4A_2-\tilde{A}\ ^2A_1$[e]		−90	+0.01		317	320	321	
$\tilde{b}\ ^4A_2-\tilde{B}\ ^2B_2$		+4	+0.03		407	393	399	
$\tilde{b}\ ^4A_2-\tilde{a}\ ^4B_1$		−93	+0.01		506	539	517	

[a]Energy above $PF_3\ \tilde{X}\ ^1A_1$.
[b]Reference 18.
[c]Reference 20.
[d]Reference 17.
[e]Electric-dipole forbidden transition.
[f]Reference 16.
[g]This work.

IV. RESULTS

Figure 1 shows four fluorescence excitation spectra of PF_3 recorded between 9–20 eV at Daresbury with an optical resolution of 0.1 nm. In Fig. 1(a) no filter was used in front of the EMI 9813 QB photomultiplier tube, while in Figs. 1(b), 1(c), and 1(d) Schott UG5, WG345 and GG420 filters were used. These filters transmit wavelengths in the range 250–400 nm, $\lambda > 335$ nm, and $\lambda > 410$ nm, respectively. The quantum efficiency of the photomultiplier tube drops dramatically for $\lambda > \sim 650$ nm. Two main conclusions can be drawn. First, these spectra show that bands in the excitation range 9–13 eV which exhibit resolved vibrational structure predominantly give rise to visible radiation with $\lambda > \sim 400$ nm, whereas those bands in the range 14–20 eV predominantly give rise to UV emission with $\lambda < \sim 400$ nm. Second, the three lowest energy bands with peaks at 9.8, 11.0, and 11.5 eV give rise to fluorescence over slightly different wavelength ranges in the visible. Specifically, noting the virtual disappearance of the 9.8 eV band with the UG5 filter [Fig. 1(b)], this band must give rise to emission at longer wavelength than the bands at 11.0 and 11.5 eV. As mentioned earlier and seen clearly from Table I, thermodynamics show that the only fragment emitter possible is the PF_2 radical. The conclusions, therefore, from this filter work are that there are at least two excited electronic states of PF_2 responsible for the emission in the photoexcitation range 9–13 eV. The emission at higher excitation energies is either due to different electronic states of PF_2, to PF, or to excited atoms.

Dispersed emission spectra between 200 and 600 nm were recorded at BESSY 1 with primary photon energies corresponding to all the major peaks in the fluorescence excitation spectrum of Fig. 1(a). The Figs. 2(a)–2(d) show the spectra recorded at energies of 9.8, 11.0, 14.4, and 16.1 eV. Figures 2(a) and 2(b) were recorded with the JYH20VIS, Figs. 2(c) and 2(d) with the JYH20UV secondary monochromator. All spectra were recorded with a 2 mm exit slit, corresponding to a resolution of 8 nm. These spectra confirm and extend the conclusions from the filter studies of Fig. 1. Specifically, the majority of the integrated emission from primary photon energies of 9.8 and 11.0 eV occurs in the visible region, with a broad unresolved peak stretching from $\sim 320-550$ nm. For an excitation energy of 11.0 eV ($E_1 = 11.0$ eV) an extra peak is observed at 300 nm which explains the presence of the 11.0 eV band with the UG5 filter in Fig. 1(b). We show later that the peak at 325 nm in Fig. 2(a) is probably due to weak second-order radiation from the primary monochromator (i.e., second order of 19.6 eV) giv-

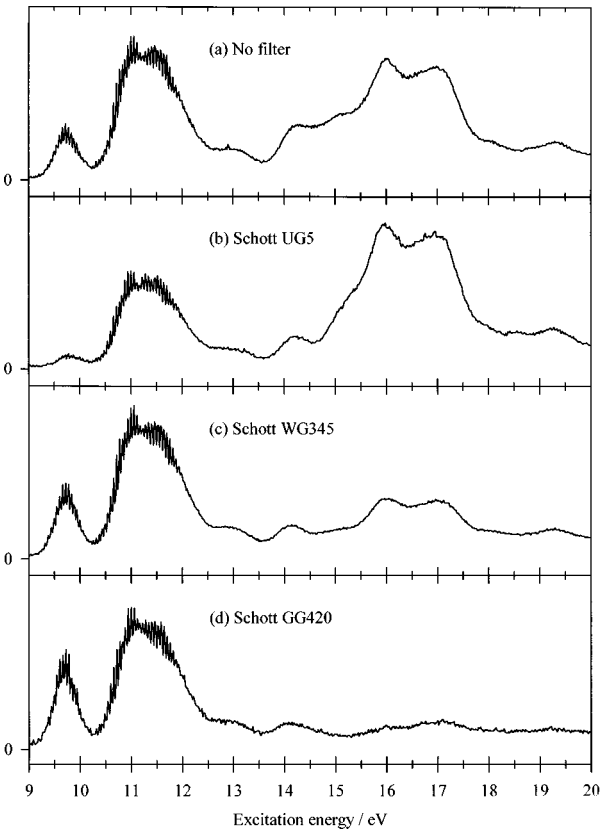

FIG. 1. Fluorescence excitation spectra of PF_3 between 9 and 20 eV recorded at the Daresbury synchrotron source with an optical resolution of 0.1 nm, equivalent to a resolution of ~0.01 eV at 12 eV. The spectra are recorded in the flux-normalized mode, and the background fluorescence has been subtracted. In (b), (c), and (d), Schott UG5, WG345, and WG420 filters, respectively, are used in front of the EMI 9813 QB photomultiplier tube. The effective range over which fluorescence is collected is therefore (a) 190–650 nm, (b) 250–400 nm, (c) 335–650 nm, and (d) 410–650 nm.

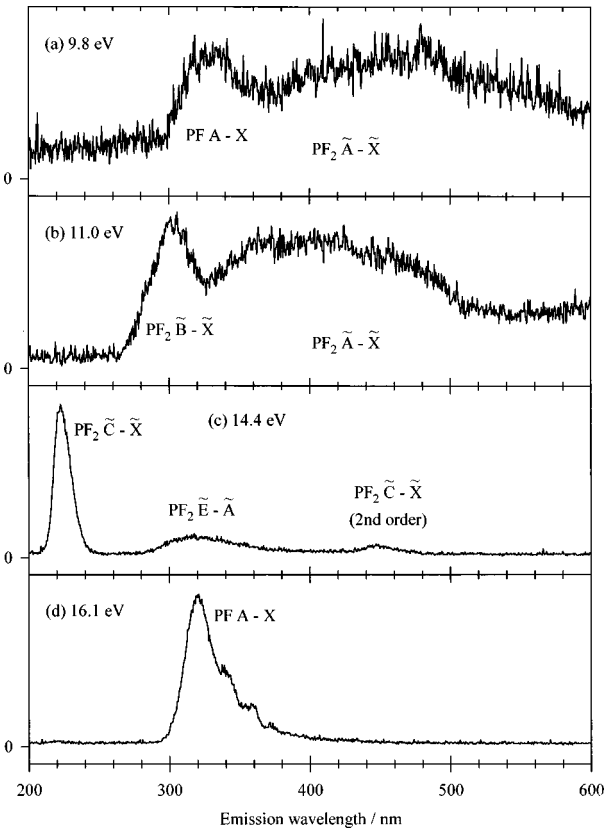

FIG. 2. Dispersed emission spectra for PF_3 photoexcited at (a) 9.8, (b) 11.0, (c) 14.4, and (d) 16.1 eV. The optical resolution was ~8 nm. A Jobin Yvon H20VIS monochromator was used for (a) and (b), an H20UV for (c) and (d). No attempt has been made to allow for the variation of sensitivity of the detection system with wavelength, but the former instrument has more sensitivity at $\lambda > \sim 450$ nm. Assignments of the main emission bands are given. Note that the band at 325 nm in (a) arises due to second-order radiation from the primary monochromator.

ing rise to PF $A-X$ emission. For primary photon energies of 14.4 and 16.1 eV, the dispersed spectrum changes dramatically. The broad visible band is lost, and new bands below 400 nm appear. For $E_1 = 14.4$ eV, two new bands are observed with peaks at 222 and 325 nm, and a much weaker band at 444 nm which is due to second-order radiation from the secondary monochromator (i.e., 2×222 nm). For $E_1 = 16.1$ eV, these three bands disappear and are replaced by a new band peaking at 322 nm with shoulders at 340 and 360 nm. It should be noted that both the low-wavelength threshold and width of the 322–325 nm bands differs in Figs. 2(c) and 2(d), and so they definitely represent different emissions.

Figures 3(a)–3(c) show action spectra where the primary monochromator is scanned for detection of fluorescence at a fixed emission wavelength, $\lambda_2 \pm 8$ nm. Spectra were recorded at λ_2 values of 222, 300, and 322, corresponding to the main peaks observed in the dispersed emission spectra. In Sec. V we show that these peaks correspond primarily to (a) PF_2 $\tilde{C}\,^2A_1 - \tilde{X}\,^2B_1$, (b) PF_2 $\tilde{B}\,^2B_2 - \tilde{X}\,^2B_1$ and $\tilde{E}\,^2B_1 - \tilde{A}\,^2A_1$, and (c) PF_2 $\tilde{E}\,^2B_1 - \tilde{A}\,^2A_1$ and PF $A\,^3\Pi - X\,^3\Sigma^-$ emissions, respectively. Note in Fig. 3(c) that the threshold for PF $A\,^3\Pi$ production occurs at 14.8 ± 0.2 eV which agrees well with the thermodynamic threshold for production of PF $A\,^3\Pi + 2F$ of 14.68 eV.

Lifetimes of the emissions induced in PF_3 at excitation energies of 9.8, 11.0, 14.4, and 16.1 eV were measured using the single-bunch mode of the BESSY 1 source. As mentioned in Sec. II, these experiments used a red-sensitive photomultiplier tube with a risetime of ~1.5 ns, and the JYH20VIS secondary monochromator with a 2 mm exit slit. The time-resolved decays at excitation energies of 9.8, 11.0, and 16.1 eV were all flat across the 200 ns range of the time-to-amplitude converter, irrespective of whether λ_2 was set to zero order or to the peak wavelength in the dispersed emission spectrum. We conclude that the lifetimes of these emissions are much longer (i.e., $\tau > \sim 500$ ns) than can be measured with the BESSY 1 source which has a time between pulses of only 208 ns. The decays at an excitation energy of 14.4 eV with λ_2 set to (a) 222 and (b) 325 nm are shown in Fig. 4. The lifetimes were analyzed both by single- and double-exponential functions, with deconvolution of the prompt signal (no gas, $\lambda_1 = \lambda_2 = 0$) as described in Sec. II. In choosing the best fit, consideration was given to the pairwise correlation functions of the fitted parameters, and to ensure both that the residuals of the fit showed nonsystematic trends and that the fitted background agreed with

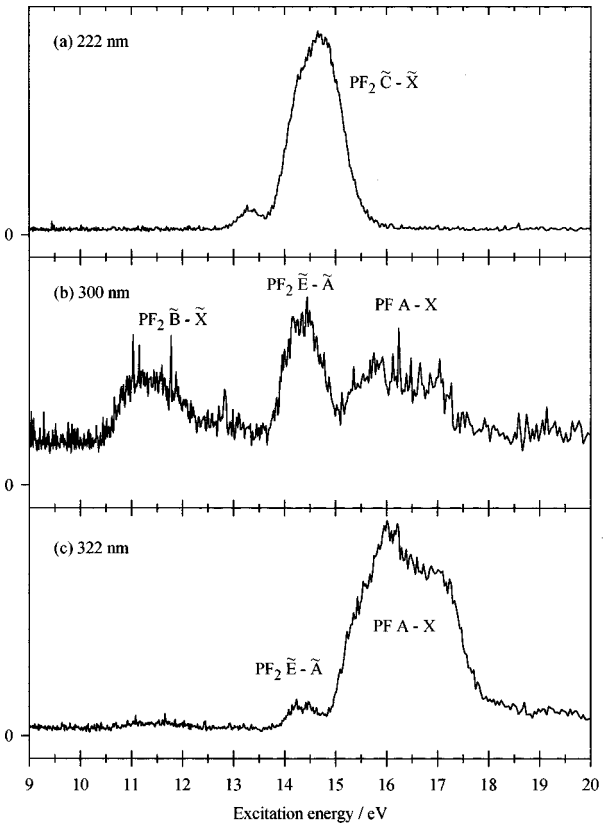

FIG. 3. Action spectra of PF_3 recorded at the BESSY 1 synchrotron source between 9 and 20 eV with detection of the fluorescence at (a) 222, (b) 300, and (c) 322 nm. These wavelengths correspond primarily to (a) PF_2 $\tilde{C}\ ^2A_1-\tilde{X}\ ^2B_1$, (b) PF_2 $\tilde{B}\ ^2B_2-\tilde{X}\ ^2B_1$ and $\tilde{E}\ ^2B_1(^2\Pi)-\tilde{A}\ ^2A_1(^2\Pi)$, and (c) PF_2 $\tilde{E}\ ^2B_1(^2\Pi)-\tilde{A}\ ^2A_1(^2\Pi)$ and PF $A\ ^3\Pi-X\ ^3\Sigma^-$ emissions, respectively. In all cases the optical resolution is 0.3 nm, the λ_2 values are defined to ± 8 nm, and the fluorescence has not been normalized to the vacuum-UV radiation from the primary monochromator.

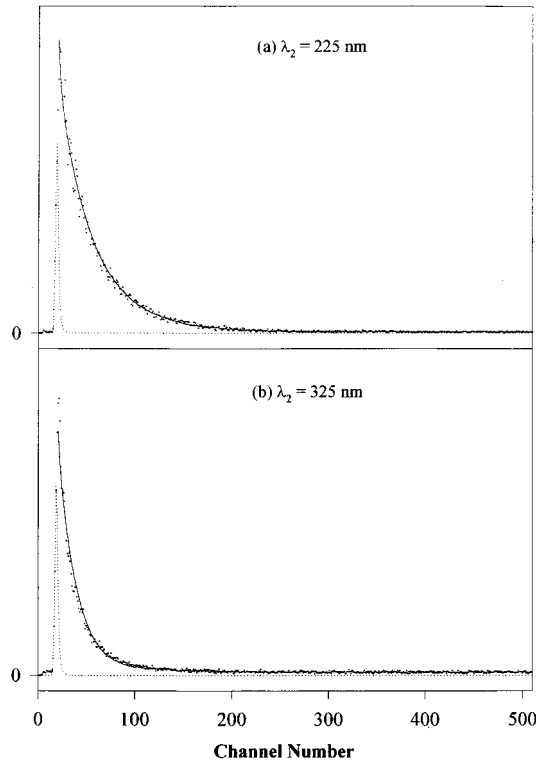

FIG. 4. Decay of the fluorescence following excitation of PF_3 at 14.4 eV with single-bunch, pulsed radiation from the BESSY 1 synchrotron source. The secondary monochromator is set to (a) $\lambda_2=225\pm 8$, (b) $\lambda_2=325\pm 8$ nm, respectively. Each spectrum shows the experimental data points, the prompt signal (dashed line), and the fit to the data (solid line) using the method described in Sec. II. The time calibration is 0.3947 ns per channel. In (a) emission is due to the bent $\tilde{C}\ ^2A_1$ state of PF_2 and the decay fits best to a single-exponential function with $\tau=14.7\pm 0.1$ ns. In (b) emission is due to the linear $\tilde{E}\ ^2B_1(^2\Pi)$ state of PF_2, and the decay again fits best to a single-exponential function with $\tau=7.9\pm 0.1$ ns.

its experimental value. Both decays fit best to single-exponentials with $\tau=14.7\pm 0.1$ and 7.9 ± 0.1 ns in Figs. 4(a) and 4(b) respectively. These results are summarized in Table IV.

V. DISCUSSION

First we consider the assignment of the peaks in the fluorescence excitation spectrum (Fig. 1). Three bands are observed at low energy which show resolved vibrational structure with peak energies of 9.75, 11.05, and ~11.55 eV. We have shown that fluorescence can only be due to the PF_2 fragment, but at this stage we just regard fluorescence in this radical as a signature of vacuum-UV absorption in the PF_3 molecule. As described before,[5] these bands show a constant vibrational spacing between the peaks of 57 ± 3 meV (458 ± 24 cm^{-1}) which is assigned to the ν_2 bending frequency in the upper state of these transitions. Since the appearance of these bands is very similar to that of the first band of the He–I or Ne–I photoelectron spectrum,[8] they can be assigned to transitions to Rydberg states that converge on the ground state of PF_3^+. Approximate values for the quantum defects of ns, np, and nd orbitals are predicted for Rydberg orbitals centered on a P atom to be $\delta=\sim 1.9$, 1.5, and 0.1,[33] respectively. By also using a vertical IP for the $(8a_1)^{-1}$ ionization of PF_3 of 12.25 eV,[8] we have assigned these bands as most likely due to transitions to the $(8a_1)^{-1}np$ $(n=4,5,6)$ Rydberg states of PF_3. This yields experimental δ values of 1.67 (for $4p$), 1.63 ($5p$), and 1.59 ($6p$). Transitions to these Rydberg states from the ground state are electric-dipole allowed. However, we now note that an alternative assignment of these bands to transitions to the $(8a_1)^{-1}ns$ $(n=4,5,6)$ Rydberg states, as suggested by Au *et al.*[10] is also allowed by electric-dipole selection rules, and would also yield quantum defects for these s Rydberg orbitals which are compatible with predictions. To the best of our knowledge, these two assignments cannot be distinguished. Using Franck–Condon calculations based on the intensity distribution of the vibrational structure in each band,[5] it has been possible to estimate the change in FPF bond angle between the ground state and these Rydberg states of PF_3 to be $14\pm 1°$. Hence the bond angle of both these Rydberg states and the ground state of PF_3^+ to which they converge is $112\pm 1°$, which is less than the 120° which would pertain if $PF_3^*/PF_3^+\tilde{X}\ ^2A_1$ were planar. This geometry has been confirmed by *ab initio* calculations.[5,34] It is much more difficult to make definitive

TABLE IV. Lifetimes of emission bands observed from vacuum-UV excitation of PF_3 in the range 9–20 eV.

E_1 /eV	λ_2 /nm (±8 nm)	τ_n /ns	A_n	Reduced χ^2	Emitter(s)
9.8	0	flat decay[a]			
9.8	450	flat decay			PF_2 $\widetilde{A}\ ^2A_1(^2\Pi)$[b]
11.0	0	flat decay			
11.0	300	flat decay			PF_2 $\widetilde{B}\ ^2B_2$
11.0	450	flat decay			PF_2 $\widetilde{A}\ ^2A_1(^2\Pi)$
14.4	0	3.7±0.2	1.0±0.1	1.26	
		15.6±0.2	0.7±0.1		
14.4	222	14.7±0.1		1.55	PF_2 $\widetilde{C}\ ^2A_1$
14.4	325	7.9±0.1		1.70	PF_2 $\widetilde{E}\ ^2B_1(^2\Pi)$[b]
16.1	0	flat decay			
16.1	322	flat decay			PF $A\ ^3\Pi$

[a]With the signal-to-noise ratio of our spectra, we assume that a flat decay implies $\tau > \sim 500$ ns.
[b]Notation for linear or near-linear states given in both C_{2v} and $D_{\infty h}$ symmetry.

assignments of the higher-energy peaks in the fluorescence excitation spectrum mainly because the bands are broader and multiple assignments are possible. The peaks must correspond to Rydberg states of PF_3 converging on excited electronic states of PF_3^+. However, it is worth noting that above ~ 12 eV there seems only to be partial agreement between our fluorescence excitation spectrum and the photoabsorption spectrum recorded by pseudo-photon dipole (e,e) spectroscopy.[10] This implies that photodissociation to fluorescing states of PF_2 or PF is not the major dissociation channel of PF_3^*, and we should note that our experiment is not sensitive to dissociation of PF_3^* to ground state PF_2 or PF.

We now consider assignment of the dispersed emission spectra of Fig. 2. For excitation energies below 13 eV, we have commented earlier that for thermodynamic reasons PF cannot be the emitter of the UV/visible bands, and therefore the emissions must be due to electronic transitions in the PF_2 radical. Since the only valence transition observed in PF_2 prior to this work was the band observed by Zhao and Setser (ZS) in a flowing PF_3/Ar discharge source,[16] the assignment of which is uncertain, we are heavily reliant on the predictions of theory to assign our spectra. Two general factors have guided our assignment. The first is to note the very different conditions under which PF_2^* is produced in the two experiments. The pressure in the ZS experiment is ~ 1 Torr, implying vibrational relaxation is complete, and hence emission is only observed from the lowest vibrational levels of the emitting PF_2^* state. By contrast, since we are working under much lower pressure conditions, emission can be observed prior to vibrational relaxation. Furthermore, since PF_2^* is formed by photodissociation of higher-lying Rydberg states of PF_3, it is quite possible for PF_2^* to be produced over a wide range of vibrational levels. The extent of PF_2^* vibrational excitation will depend upon the dynamics of the photodissociation, but excitation in ν_2 and/or ν_1 will be especially likely if there is a large change in FPF bond angle and/or P–F bond length between PF_3^* and PF_2^*. At this stage we should note the large change in ϑ_{FPF} and R_{P-F} predicted for many of the states of PF_2^* (Table II) from the calculated values in PF_3^* ($\vartheta_{FPF}=109°$, $R_{P-F}=1.50$ Å).[5] The situation is therefore very similar to that of the photodissociation of the boron $3s$ and $3p$ Rydberg states of BF_3 producing the $\widetilde{A}\ ^2B_1$ and $\widetilde{B}\ ^2A_1$ states of BF_2 over a wide range of ν_2 bending vibrational levels.[35] The second point is that of all the electronic transitions in Table III that could give rise to PF_2 emission in the UV/visible, it is the ones with small $|\Delta\vartheta|$ and/or small $|R_e|$ that are most likely to be observed, since they will have all their vibrational bands with large Franck–Condon factors localized into a narrow region of energy. Conversely, transitions with large $|\Delta\vartheta|$ or $|R_e|$, especially those that are electric-dipole or spin–forbidden, are unlikely to be observed.

The emission spectrum observed at an excitation energy of 9.8 eV [Fig. 2(a)] shows a very broad unresolved band between ~ 320 and 550 nm. We assign this spectrum to the $\widetilde{A}\ ^2A_1-\widetilde{X}\ ^2B_1$ transition in PF_2, a near-linear to bent transition between the two Renner–Teller components of $^2\Pi$ symmetry.[18] Calculations predict the origin of this band to lie between 500 and 650 nm, but if the $\widetilde{A}\ ^2A_1$ state is produced vibrationally hot by photodissociation of the $(8a_1)^{-1}4s/4p$ Rydberg state of PF_3, emission to the ground state of PF_2 will occur over a wide range of wavelengths, with much of the emission having $\lambda < \lambda_e$. The broad nature of the spectrum is compatible with this assignment, and we note that the sensitivity of the apparatus decreases rapidly for $\lambda > \sim 550$ nm. The weak peak centered on 325 nm has exactly the same low-wavelength threshold and width as the dispersed spectrum at 16.1 eV [Fig. 2(d)]. This spectrum is due to PF $A\ ^3\Pi-X\ ^3\Sigma^-$ emission (see later), and is also observed at an excitation energy of 19.6 eV. We therefore assign this peak in Fig. 2(a) to PF $A-X$ emission caused by second-order radiation from the primary monochromator.

Photodissociation of the $(8a_1)^{-1}5s/5p$ Rydberg state of PF_3 at 11.0 eV produces the same broad visible band, but also a new narrower band with a maximum at 300 nm [Fig. 2(b)]. From Table I, the only new electronic states of PF_2 that could be responsible for this emission are the bent $\widetilde{B}\ ^2B_2$ or the linear $\widetilde{a}\ ^4B_1$ states. Noting that the $\widetilde{a}-\widetilde{X}$ transition in

PF_2 is both spin–forbidden and has a very large $|\Delta\vartheta|$, we assign this band to the electric-dipole-forbidden $\tilde{B}\,^2B_2-\tilde{X}\,^2B_1$ transition. This transition has a much smaller $|\Delta\vartheta|$ value of only 14°, and the dipole-forbidden nature of the transition can explain the relatively long lifetime ($\tau > \sim 500$ ns) of the $\tilde{B}\,^2B_2$ state. Our assignment is in apparent contradiction with previous assignments[17–19] of the ZS spectrum.[16] This point is discussed below.

For an excitation energy of 14.4 eV, bands are observed at 222 and 325 nm which are both relatively narrow (compared to PF_2 $\tilde{A}-\tilde{X}$) and whose upper states have lifetimes less than 20 ns. We make the fundamental assumption that both these bands must be due to allowed electronic transitions in PF_2 with relatively small geometry changes between the two electronic states. Furthermore, since the lifetimes of the two states are clearly not the same, different excited electronic states of PF_2 must be responsible for these two emissions. Noting that the $\tilde{C}\,^2A_1$ to $\tilde{G}\,^2A_2$ states of doublet symmetry and the $\tilde{b}\,^4A_2$ state of quartet symmetry are now energetically open, and by comparing the predictions of λ_e with experiment, we assign these two bands to the $\tilde{C}\,^2A_1-\tilde{X}\,^2B_1$ and $\tilde{E}\,^2B_1(^2\Pi)-\tilde{A}\,^2A_1(^2\Pi)$ transitions, respectively. We believe that, with the possible exception of the higher wavelength band which may be due to $\tilde{D}\,^2B_2-\tilde{B}\,^2B_2$, these are the only assignments that satisfy the criteria we have imposed. Note that both the $\tilde{C}-\tilde{X}$ and $\tilde{E}-\tilde{A}$ transitions are dipole allowed, and the lifetime of the $\tilde{C}\,^2A_1$ state (14.7 ns) agrees excellently with the prediction of Cai (16 ns).[20]

We believe that these assignments of the four emissions bands in PF_2 ($\tilde{A}-\tilde{X}$, $\tilde{B}-\tilde{X}$, $\tilde{C}-\tilde{X}$, and $\tilde{E}-\tilde{A}$) are self consistent, and satisfy all the criteria described earlier. However, our results necessarily beg the question of the assignment of the spectrum observed by Zhao and Setser.[16] Both from the predicted energy and from Franck–Condon calculations of the predicted intensity distribution, three theoretical studies[17–19] have assigned the ZS spectrum to the $\tilde{B}\,^2B_2-\tilde{X}\,^2B_1$ transition in PF_2. Furthermore, the Franck–Condon analysis[19] had to assume that the radical was formed in the electrical discharge with an approximate Boltzmann vibrational temperature of 298 K. Due to the bond angle change between these two states of PF_2 ($\sim 14°$), the bands with strongest Franck–Condon factor are calculated to occur at wavelengths higher than $\lambda_{0,0}$ (experimental value=421 nm),[16] the strongest being from $\nu_2' = 0$ to $\nu_2'' = 4$ at ~ 450 nm;[19] there is negligible intensity calculated at the band origin. In our experiment, however, the $\tilde{B}\,^2B_2$ state of PF_2 may be produced both vibrationally hot and inverted, especially since the FPF bond angle changes substantially from $\sim 112°$ in the $(8a_1)^{-1}5s/5p$ Rydberg state of PF_3 to $\sim 83°$ in PF_2 $\tilde{B}\,^2B_2$. Assuming vibrational relaxation does not occur, the bands with strong Franck–Condon factors in emission will be those from high ν_2' levels of $\tilde{B}\,^2B_2$ to low ν_2'' of $\tilde{X}\,^2B_1$ at wavelengths less than $\lambda_{0,0}$. We believe, therefore, that there is no inconsistency in assigning the band at 300 nm in our spectrum to PF_2 $\tilde{B}-\tilde{X}$, whilst also assigning the 420–500 nm spectrum of ZS to the same electronic transition; the difference is explained by the different methods of production of PF_2 $\tilde{B}\,^2B_2$, and especially the different vibrational populations in the two experiments.

It should be noted that both Lee *et al.*[19] and JI[17] had difficulty interpreting the $\nu_2' = 220\ \mathrm{cm}^{-1}$ vibrational assignment of ZS. JI reassigned these bands to sequence bands of the symmetric stretch, a suggestion that was questioned by Lee *et al.* It may be coincidence that $220\ \mathrm{cm}^{-1}$ is much closer to the predicted ν_2' value in the near-linear $\tilde{A}\,^2A_1(^2\Pi)$ state of PF_2, but this has led us to consider whether the $\tilde{A}-\tilde{X}$ transition could be contributing to the ZS spectrum. The origin of the $\tilde{A}-\tilde{X}$ transition is calculated to occur between 500 and 650 nm,[17,18] and in the ZS experiment bands of this transition with appreciable Franck–Condon activity will lie to longer wavelength of λ_e from $\nu_A' = 0$ to high levels of ν_X''. We therefore agree with the conclusion of Lee *et al.* that the $\tilde{A}-\tilde{X}$ transition in PF_2 cannot be contributing to the spectrum observed by ZS under their experimental conditions. Note, however, that under our very different experimental conditions, if the $\tilde{A}\,^2A_1$ state is produced vibrationally hot and inverted, as seems likely given the large bond angle change between the PF_3 Rydberg states and PF_2 $\tilde{A}\,^2A_1$, PF_2 $\tilde{A}-\tilde{X}$ emission will be produced over a very wide range of wavelengths with much of the emission occurring below λ_e. The assignments of emissions to PF_2 $\tilde{A}-\tilde{X}$ and $\tilde{B}-\tilde{X}$ under our experimental conditions at shorter wavelengths than those of the calculated bond origins is therefore entirely self-consistent.

We now consider the emission from PF_3 excited at 16.1 eV. All the PF_2 bands disappear, and a new band is observed with a low-wavelength threshold of 295 nm, a peak at 322 nm, and shoulders at 340 and 360 nm. By comparison with a published spectrum of He* ($2\,^3S$) excitation of PF_3,[36] we assign this emission to vibrational bands in PF $A\,^3\Pi-X\,^3\Sigma^-$. The maximum at 322 nm corresponds to bands with $\Delta v = 2$, 3, and 4 which have the largest Franck–Condon factors to $v'' = 0$. The shoulder around 340 nm is essentially due to bands with $\Delta v = 0$, and the shoulder at 360 nm to bands with $\Delta v = -2$. The long lifetime assumed from our single-bunch study ($\tau > \sim 500$ ns) is consistent with the recent measurement of the PF $A\,^3\Pi$ state lifetime of $4.2 \pm 0.2\ \mu$s.[31] Our experiment gives no information on whether the other product of the photodissociation is F_2 or 2F. Both channels are energetically open at an excitation energy of 16.1 eV. However, we should note from the action spectrum [Fig. 3(c)] that the experimental threshold for production of PF $A\,^3\Pi$, 14.8 ± 0.1 eV, lies very close to the thermodynamic threshold of PF $A\,^3\Pi + 2$F of 14.68 eV. Direct dissociation of singlet Rydberg states of PF_3 to PF ($A\,^3\Pi$) $+ F_2$ ($X\,^1\Sigma_g^+$) is formally spin–forbidden. Conversely, if photodissociation occurs sequentially in two steps [i.e., $PF_3^* \rightarrow PF_2^* + F(^2P) \rightarrow PF(A\,^3\Pi) + F(^2P) + F(^2P)$] via an excited state of PF_2 with doublet symmetry, these processes are both spin allowed. The fact that the experimental threshold for production of PF $A\,^3\Pi$ does lie close to the thermochemical energy of PF $A\,^3\Pi + 2$F suggests that photodissociation occurs sequentially in two steps via an excited state

of PF_2 with doublet spin symmetry. For identical reasons, a similar mechanism was deduced in our recent SiF_4 study for photodissociation of Rydberg states of SiF_4 to SiF_2^* ($\tilde{A}\,^1B_1$ or $\tilde{a}\,^3B_1$), with F+F being inferred as the other products of the two-step, sequential dissociation.[4]

With these assignments, we are now able to interpret the action spectra of Fig. 3. Detection at $\lambda_2 = 222 \pm 8$ nm [Fig. 3(a)] corresponds to isolation of the PF_2 $\tilde{C}-\tilde{X}$ emission band. With a threshold energy of $\sim$12.9 eV, peaks are observed at 13.3 and 14.6 eV which must correspond to Rydberg states of PF_3 that photodissociate to the $\tilde{C}\,^2A_1$ state of PF_2. These results are consistent with thermochemistry; the energy of the $\tilde{C}\,^2A_1$ state of PF_2 is calculated to lie lower than 12.9 eV, at 11.07 eV (Table I). Detection at $\lambda_2 = 300 \pm 8$ nm [Fig. 3(b)] corresponds to isolation of the PF_2 $\tilde{B}-\tilde{X}$ and the tail of the $\tilde{E}-\tilde{A}$ emissions. Thus a peak is observed at 11 eV with a threshold of $\sim$10.5 eV, corresponding to excitation of the $(8a_1)^{-1}5p,6p$ Rydberg states of PF_3 which dissociate to the $\tilde{B}\,^2B_2$ state of PF_2. The second peak at 14.4 eV must correspond to a higher Rydberg state of PF_3 that photodissociates to the $\tilde{E}\,^2B_1(^2\Pi)$ pseudo-linear state of PF_2. Detection at $\lambda_2 = 322 \pm 8$ nm [Fig. 3(c)] corresponds to isolation of the PF_2 $\tilde{E}-\tilde{A}$ and PF $A-X$ bands. Emission at this wavelength from the $\tilde{A}\,^2A_1$ and $\tilde{B}\,^2B_2$ states of PF_2 is, by comparison, much weaker, and therefore no peaks in the action spectrum are observed below 13 eV. Peaks are observed at 14.4 and 16.1 eV, corresponding to Rydberg states of PF_3 that photodissociate to the $\tilde{E}\,^2B_1(^2\Pi)$ state of PF_2 and the $A\,^3\Pi$ state of PF, respectively.

The dispersed emission spectra for photoexcitation energies greater than 16.1 eV yield the same spectrum as observed in Fig. 2(d), i.e., PF $A-X$ emission dominates. This confirms another result from the action spectrum at $\lambda_2 = 322$ nm [Fig. 3(c)] that emission at this wavelength is still present for photon energies up to 20 eV. Specifically, at 19.6 eV the $A\,^3\Pi$ state of PF is the main emitter. This is therefore confirmation that the peak observed at 325 nm in the dispersed spectrum for photoexcitation of PF_3 at 9.8 eV [Fig. 2(a)] is due to PF $A-X$ produced by second-order radiation of the primary monochromator.

VI. CONCLUSIONS

Using monochromatised radiation from the Daresbury, UK synchrotron as the source of tunable vacuum-UV photons, we have made an extensive study of the vacuum-UV fluorescence spectroscopy of PF_3 in the range 9–20 eV. Transitions to the three lowest Rydberg states of PF_3, converging on the ground state of PF_3^+, show resolved vibrational structure in the ν_2 umbrella mode. From a Franck–Condon analysis of the structure, the FPF bond angle in PF_3 is calculated to increase by $\sim 14 \pm 1°$ upon photoexcitation. The use of optical filters in the fluorescence excitation spectrum has shown that at least three excited electronic states of the PF_2 radical are responsible for the induced emission. Dispersed emission and action spectra, recorded at the BESSY 1 source in Berlin, have been shown to be more powerful techniques to determine the precise nature of the emitter(s). From these dispersed spectra, it has been shown that four different decay channels are observed: (a) PF_2 $\tilde{A}\,^2A_1-\tilde{X}\,^2B_1$ fluorescence in the wide range 320–550 nm for photon energies around 9.8 eV, (b) PF_2 $\tilde{A}-\tilde{X}$, and $\tilde{B}\,^2B_2-\tilde{X}\,^2B_1$ fluorescence at $\sim$300 nm for photon energies around 11.0 eV, (c) PF_2 $\tilde{C}\,^2A_1-\tilde{X}\,^2B_1$ and $\tilde{E}\,^2B_1(^2\Pi)-\tilde{A}\,^2A_1$ fluorescence at $\sim$222 and 325 nm, respectively, for photon energies around 14.4 eV, and (d) PF $A\,^3\Pi-X\,^3\Sigma^-$ fluorescence between 300–380 nm for photon energies between 16 and 20 eV. Our experiments give no information on quantum yields for production of these excited states of PF_2 and PF. Using the single-bunch mode of the BESSY 1 source, we have measured the lifetimes of the bent $\tilde{C}\,^2A_1$ and linear $\tilde{E}\,^2B_1(^2\Pi)$ states of PF_2 to be 14.7 and 7.9 ns, respectively, and we note that the range of lifetimes which can be measured in this way is relatively narrow, $\sim$5–150 ns. The ability to define the wavelength of the emission with the secondary monochromator when more than one emitter was excited was particularly important, and meant that the lifetimes of the $\tilde{C}\,^2A_1$ and $\tilde{E}\,^2B_1$ states of PF_2 could be measured independently. Finally, we should note that, unlike previous studies,[1–4] the assignment of the emission bands in PF_2 was heavily dependent on the results of high quality *ab initio* calculations. We hope that this work stimulates higher-resolution experimental studies on the electronic spectroscopy of the PF_2 free radical.

ACKNOWLEDGMENTS

We thank EPSRC and the Daresbury Laboratory for a Research Grant, Research Studentships (KJB, DPS) and a CASE award (KJB). H.B. thanks the Deutsche Forschungsgemeinschaft for a PostDoctoral Fellowship. The EU Training and Mobility of Researchers programme (contract number ERBFMGE-CT-950031) and the British Council (ARC bilateral programme with Germany, contract number 707) are also acknowledged for funding. Finally, we thank Dr. M. A. Hayes of the Daresbury Laboratory for programming and advice with the use of the lifetime fitting program FLUOR.

[1] H. Biehl, J. C. Creasey, D. M. Smith, R. P. Tuckett, K. R. Yoxall, H. Baumgärtel, H. W. Jochims, and U. Rokland, J. Chem. Soc. Faraday Trans. **91**, 3073 (1995).
[2] H. Biehl, D. M. Smith, R. P. Tuckett, K. R. Yoxall, H. Baumgärtel, H. W. Jochims, and U. Rokland, Mol. Phys. **87**, 1199 (1996).
[3] H. Biehl, K. J. Boyle, R. P. Tuckett, H. Baumgärtel, and H. W. Jochims, Chem. Phys. **214**, 367 (1997).
[4] H. Biehl, K. J. Boyle, D. M. Seccombe, D. M. Smith, R. P. Tuckett, K. R. Yoxall, H. Baumgärtel, and H. W. Jochims, J. Chem. Phys. **107**, 720 (1997).
[5] R. P. Tuckett and P. J. Knowles, Chem. Phys. Lett. **261**, 486 (1996).
[6] I. H. Hiller and V. R. Saunders, Trans. Faraday Soc. **66**, 2401 (1970); P. J. Bassett, D. R. Lloyd, I. H. Hillier, and V. R. Saunders, Chem. Phys. Lett. **6**, 253 (1970).
[7] Y. Morino, K. Kuchitsu, and T. Moritani, Inorg. Chem. **8**, 867 (1969).
[8] J. P. Maier and D. W. Turner, J. Chem. Soc. Faraday Trans 2. **68**, 711 (1972).
[9] D. J. Reynolds, E. H. van Kreef, and I. Powis, J. Chem. Phys. **95**, 8895 (1991).
[10] J. W. Au, G. Cooper, and C. E. Brion, Chem. Phys. **215**, 397 (1997).

[11] C. E. Humphries, A. D. Walsh, and P. A. Warsop, Faraday Discuss. Chem. Soc. **35**, 148 (1963).
[12] M. J. McAdams and B. R. Russell, Chem. Phys. Lett. **18**, 402 (1973).
[13] M. W. Chase, C. A. Davies, J. R. Downey, D. J. Frurip, R. A. MacDonald, and A. N. Syverud, J. Phys. Chem. Ref. Data Suppl. **14** (1985).
[14] A. E. Douglas and M. Frackowiak, Can. J. Phys. **40**, 832 (1962).
[15] L. Latifzadeh and K. Balasubramanian, Chem. Phys. Lett. **243**, 243 (1995).
[16] Y. Zhao and D. W. Setser, Chem. Phys. Lett. **210**, 362 (1993).
[17] R. D. Johnson and K. K. Irikura, Chem. Phys. Lett. **228**, 273 (1994).
[18] L. Latifzadeh and K. Balasubramanian, Chem. Phys. Lett. **228**, 463 (1994).
[19] E. P. F. Lee, D. C. Wang, and F. T. Chau, J. Phys. Chem. **100**, 19795 (1996).
[20] Z. L. Cai, J. Comput. Chem. **15**, 346 (1994).
[21] K. P. Huber and G. Herzberg, *Molecular Spectra and Molecular Structure* (Van Nostrand, New York, 1979), Vol. 4.
[22] D. M. P. Holland, J. B. West, A. A. MacDowell, I. H. Munro, and A. G. Beckett, Nucl. Instrum. Methods Phys. Res. B **44**, 233 (1989).
[23] C. M. Gregory, M. A. Hayes, G. R. Jones, and E. Pantos, Technical memorandum, Daresbury Laboratory, reference DL/SCI/TM98E (1994).
[24] S. Saito, Y. Endo, and E. Hirota, J. Chem. Phys. **85**, 1778 (1986).
[25] K. Burdet, L. Hodges, V. Dunning, and J. H. Current, J. Phys. Chem. **74**, 4053 (1970).
[26] J. D. Howe, M. N. R. Ashfold, J. W. Hudgens, and R. D. Johnson, J. Chem. Phys. **101**, 3549 (1994).
[27] V. Butcher, J. M. Dyke, A. E. Lewis, A. Morris, and A. Ridha, J. Chem. Soc. Faraday Trans. 2. **84**, 299 (1988).
[28] J. Berkowitz, J. P. Greene, J. Foropoulos, and O. M. Neskovic, J. Chem. Phys. **81**, 6166 (1984).
[29] A. D. Walsh, J. Chem. Soc. 2266 (1953).
[30] R. Colin, J. Devillers and F. Prevot, J. Mol. Spectrosc. **44**, 230 (1972).
[31] J. Xu, D. W. Setser and R. Hamman, J. Phys. Chem. **99**, 3173 (1995).
[32] Y. Zhao and D. W. Setser, J. Phys. Chem. **98**, 9723 (1994).
[33] C. E. Theodosiou, M. Inokuti, and S. T. Manson, At. Data Nucl. Data Tables **35**, 473 (1986).
[34] S. Creve and M. T. Nguyen, Chem. Phys. Lett. **273**, 199 (1997).
[35] J. C. Creasey, P. A. Hatherly, H. M. Jones, I. R. Lambert, and R. P. Tuckett, Mol. Phys. **78**, 837 (1993).
[36] U. K. Roychowdhury, S. Naxakis, J. A. Coxon, D. S. Richards, D-Z. Cao, and D. W. Setser, Chem. Phys. **118**, 427 (1987).